Supporting materials for

Zinc ion stabilized MnO₂ nanospheres for high capacity and long lifespan aqueous zinc-ion batteries

Jinjin Wang,[a] Jian-Gan Wang,[a] [*] Huanyan Liu,[a] Chunguang Wei,[b,c] Feiyu Kang[c]

[a] State Key Laboratory of Solidification Processing, Center for Nano Energy Materials, School of Materials Science and Engineering, Northwestern Polytechnical University and Shaanxi Joint Lab of Graphene (NPU), Xi'an 710072, China;

[b] Shenzhen Cubic-science Co., Ltd., Nanshan District, Shenzhen 518052, China

[c] Engineering Laboratory for Functionalized Carbon Materials and Shenzhen Key Laboratory for Graphene-based Materials, Graduate School at Shenzhen, Tsinghua University, Shenzhen 518055, China
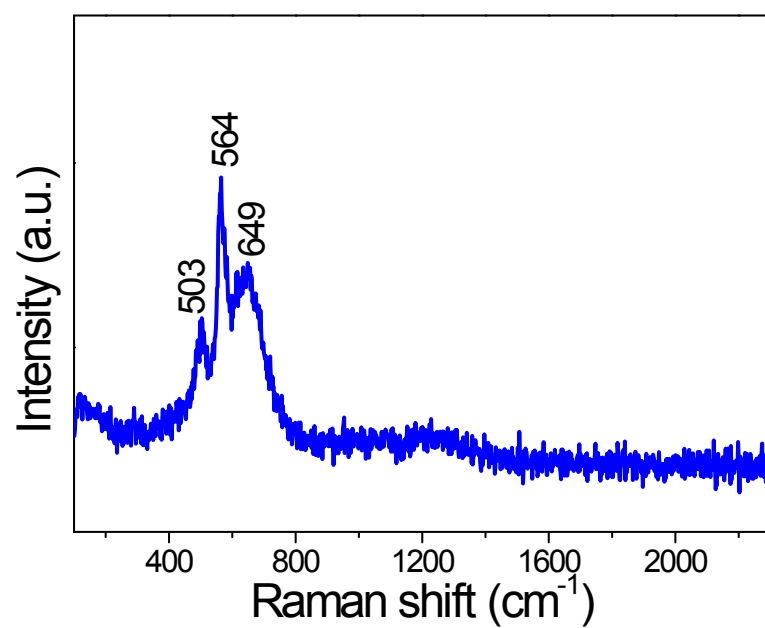
*   Corresponding email: wangjiangan@nwpu.edu.cn

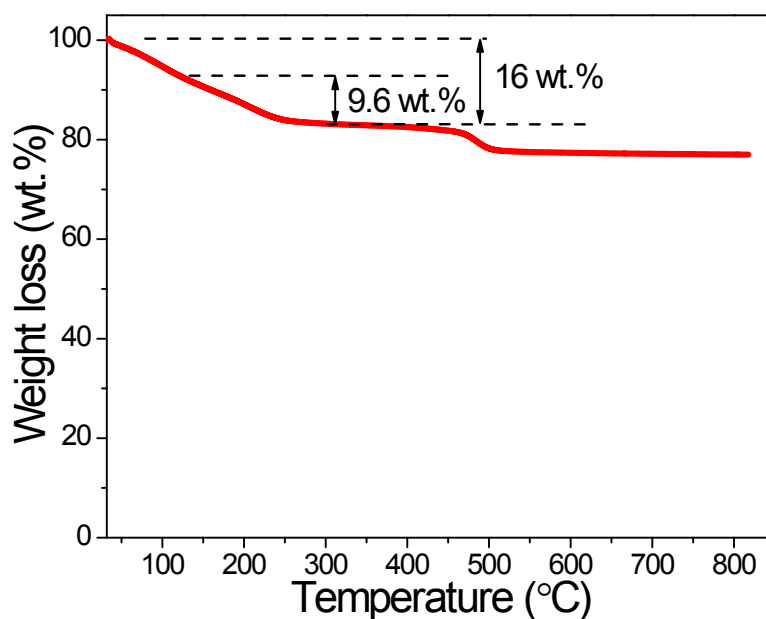Fig. S1 Raman spectra of the MnO_2 sample.

Fig. S2 TGA curve of the MnO$_2$ sample.

It is well known that MnO$_2$ with large tunnel and layered structures requires cations and water molecules to stabilize their structural framework. There are two-stage weight losses in the TGA curves. The first stage with 16 wt.% loss before 250 °C is related to the removal of surface adsorped water and structural water which is typical of layered type MnO$_2$. In general, the removal of structural water molecules starts at around 120 °C and the content can be estimated to be about 9.6 wt.%. The second stage above 420 °C corresponds to the partial reduction of manganese accompanied by oxygen evolution. The thermal behavior of MnO$_2$ is accordance with the results reported by Ghodbane et al. [ACS Appl. Mater. Interfaces, 2 (2010) 3493–3505.]
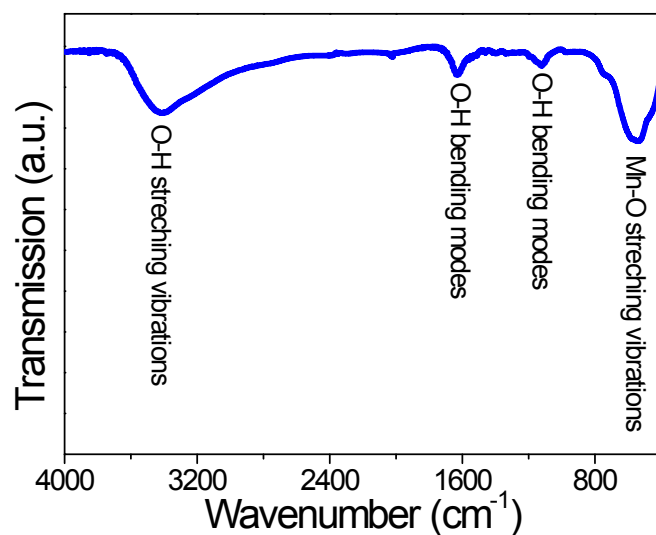
Fig. S3 FTIR spectrum of the MnO$_2$ sample.

In the spectrum, the broad adsorption peak at around 3400 cm^{-1} corresponds to the stretching vibrations of water, while the bands at 1630 and 1120 cm^{-1} are attributed to the bending modes of structural water in the framework of MnO$_2$. In addition, the strong peak at 400-800 cm^{-1} belong to the Mn-O stretching vibrations of basic [MnO$_6$] octahedra.
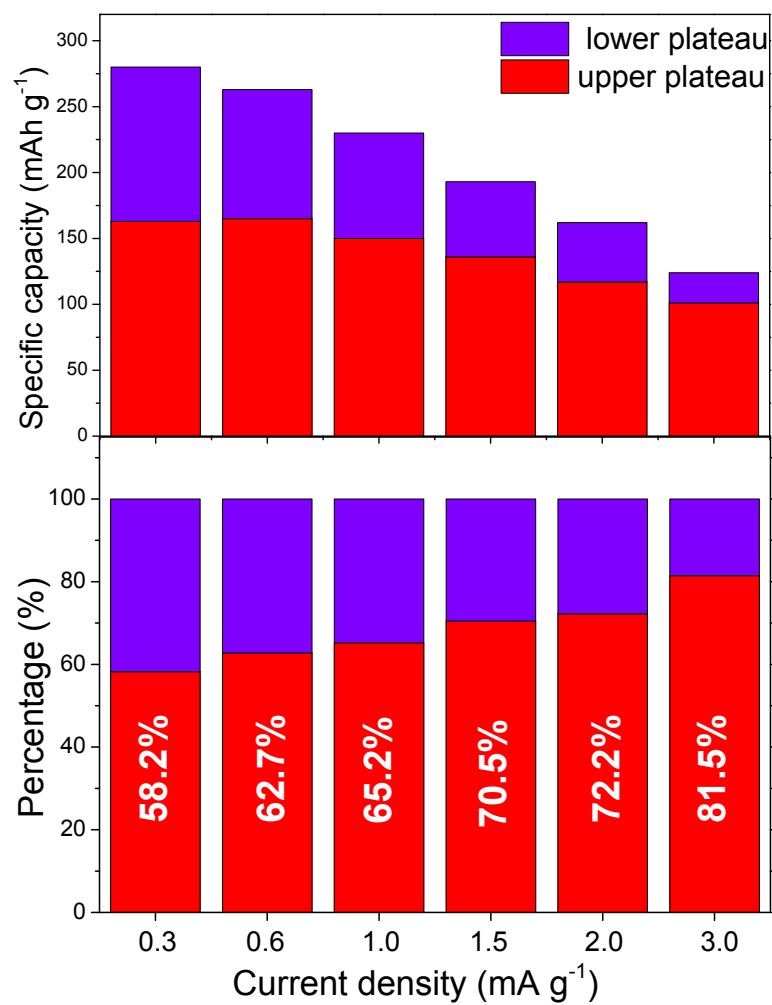
Fig. S4 A comparison of upper and lower discharge capacity at different current densities.
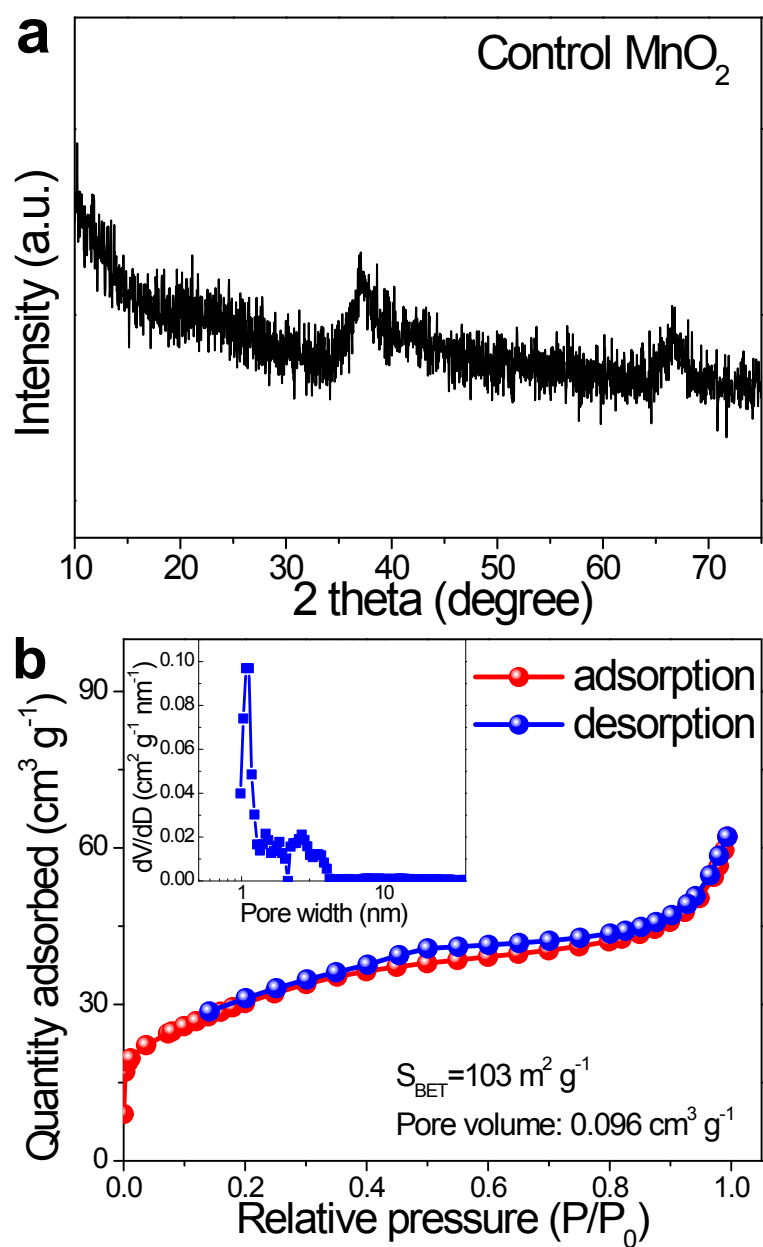
Fig. S5 (a) XRD pattern and (b) N$_2$ adsorption/desorption isotherm with the corresponding pore size distribution (inset) of the control sample of MnO$_2$.
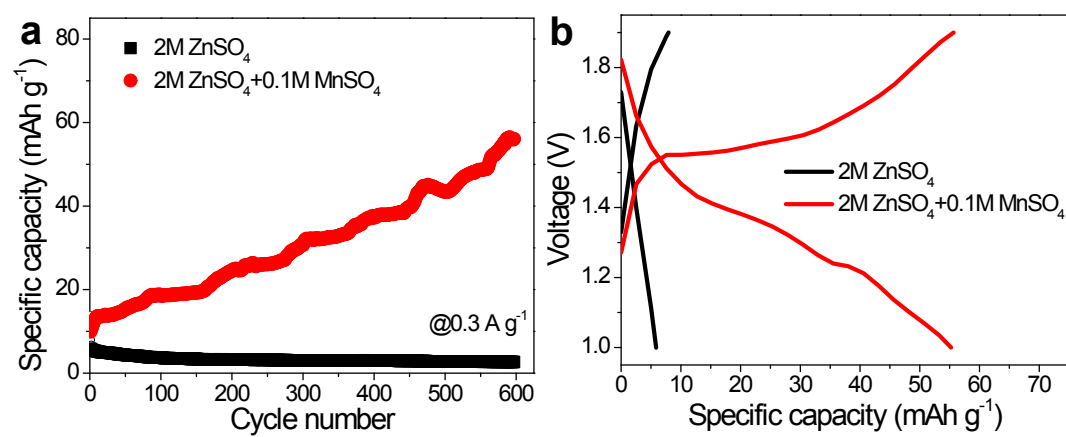
Fig. S6 (a) Cycling performance of CB electrode in $ZnSO_4$ electrolyte with and without $MnSO_4$.
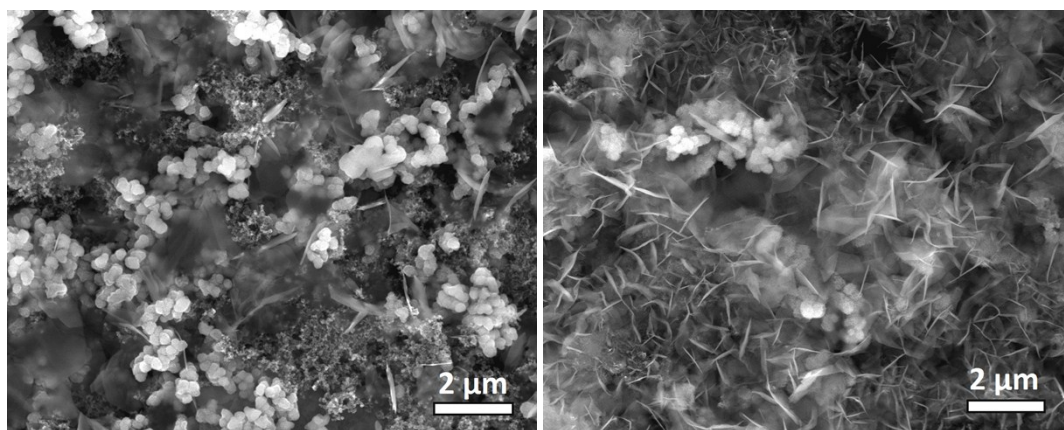(b) Charge/discharge curves of the cells after cycling test.

Fig. S7 High-resolution SEM images of the discharge cathode at (a) C state and (b) I state.
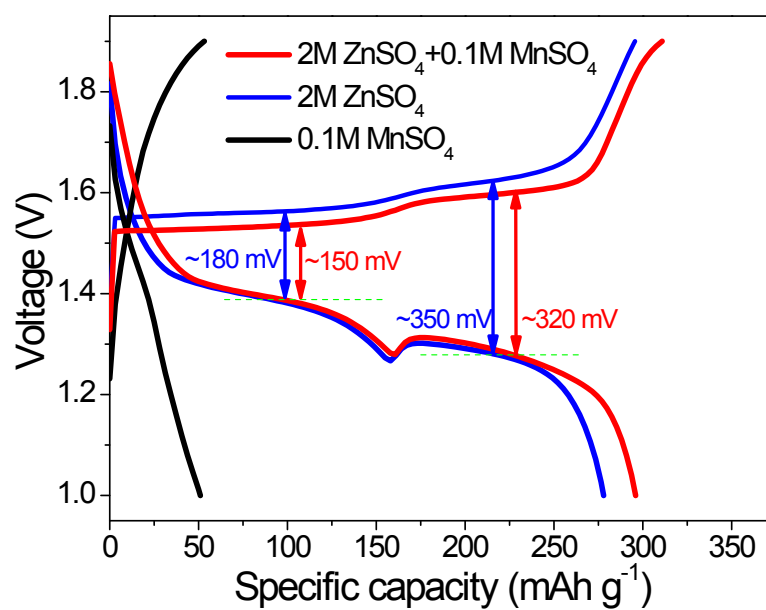
Fig. S8 Charge/discharge profiles of MnO_2 electrode in different electrolytes.
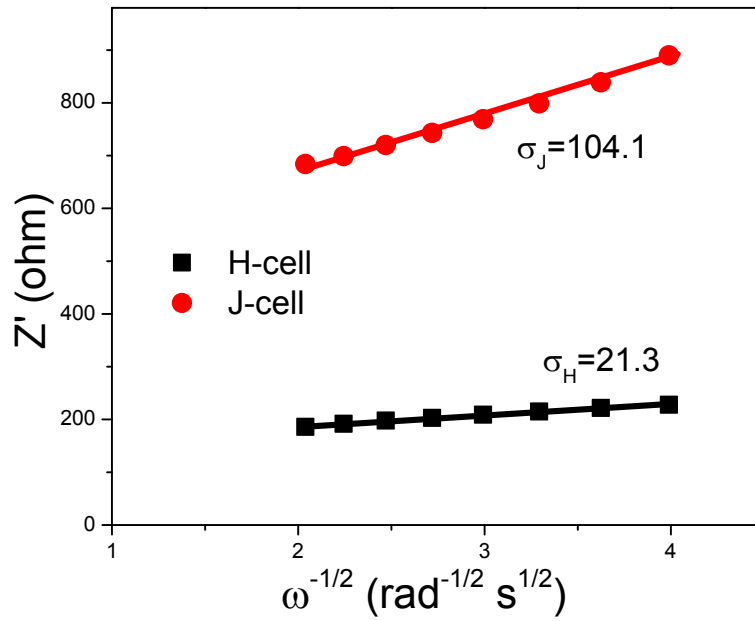
Fig. S9　A linear plot of Real resistance (Z') against angular frequencies ($\omega^{-1/2}$) in the low frequency region.

The apparent ion diffusion coefficient (D) of the ZIBs is calculated by the following equation:

$$D = \frac{R^2 T^2}{2n^4 F^4 A^2 C^2 \sigma^2}$$

Here, *R, n, T, A, F,* and *C* correspond to the gas constant, the electron number involved in the redox reaction, the absolute temperature, the geometric area of electrode, the Faraday constant, and the molar concentration of ions, respectively. σ is the Warburg coefficient, which can be calculated by plotting Z' (Ω) against $\omega^{-1/2}$ on the basis of the equation of $Z' = R_s + R_{ct} + \sigma\omega^{-1/2}$, as shown in Fig. S8.